Downloaded from orbit.dtu.dk on: Apr 25, 2025

DTU Library

Supercavity mode in a single metallic resonator

Jacobsen, Rasmus E.; Arslanagić, Samel

Published in:
Applied Physics Letters

Link to article, DOI:
10.1063/5.0174480

Publication date:
2023

Document Version
Publisher's PDF, also known as Version of record

Link back to DTU Orbit

Citation (APA):
Jacobsen, R. E., & Arslanagić, S. (2023). Supercavity mode in a single metallic resonator. *Applied Physics Letters*, *123*(22), Article 221701. https://doi.org/10.1063/5.0174480

General rights
Copyright and moral rights for the publications made accessible in the public portal are retained by the authors and/or other copyright owners and it is a condition of accessing publications that users recognise and abide by the legal requirements associated with these rights.

- Users may download and print one copy of any publication from the public portal for the purpose of private study or research.
- You may not further distribute the material or use it for any profit-making activity or commercial gain
- You may freely distribute the URL identifying the publication in the public portal

If you believe that this document breaches copyright please contact us providing details, and we will remove access to the work immediately and investigate your claim.

Applied Physics Letters

RESEARCH ARTICLE | NOVEMBER 28 2023

Supercavity mode in a single metallic resonator

Rasmus E. Jacobsen ; Samel Arslanagić

Check for updates

Appl. Phys. Lett. 123, 221701 (2023)
https://doi.org/10.1063/5.0174480

View Online
Export Citation
CrossMark

30 November 2023 10:33:23

QBLOX
Integrates all
Instrumentation + Software
for Control and Readout of
Superconducting Qubits
NV-Centers
Spin Qubits

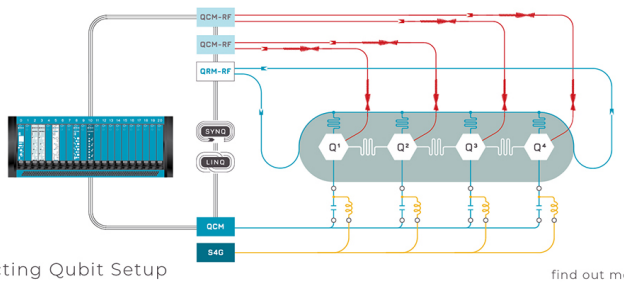

Superconducting Qubit Setup
find out more >

AIP Publishing

Applied Physics Letters ARTICLE pubs.aip.org/aip/apl

Supercavity mode in a single metallic resonator

Cite as: Appl. Phys. Lett. **123**, 221701 (2023); doi: 10.1063/5.0174480
Submitted: 31 August 2023 · Accepted: 13 November 2023 ·
Published Online: 28 November 2023

View Online Export Citation CrossMark

Rasmus E. Jacobsen[a] and Samel Arslanagić[b]

AFFILIATIONS

Department of Space Research and Technology, Technical University of Denmark, Bld. 348, Ørsteds Plads, 2800 Kgs. Lyngby, Denmark

[a]Author to whom correspondence should be addressed: rajac@dtu.dk
[b]Electronic mail: saar@dtu.dk

ABSTRACT

Bound states in the continuum are exotic nonradiating modes with very high quality factors enabling enhanced wave-matter interactions. While they typically require array-type of systems, versions of such states have been reported in single dielectric resonators, giving rise to suppressed scattering states termed supercavity modes. In this work, we experimentally demonstrate a supercavity mode in an all-metallic resonator open for probing by free-space microwaves. Our design exploits careful tailoring of the boundaries around the resonator, which supports an octupole mode fostering a significant increase in the quality factor. The main advantage of the resonator is its simplicity and robustness, and it may be utilized as a stand-alone unit for energy harvesting and sensing or as an element for advanced functional material designs.

Published under an exclusive license by AIP Publishing. https://doi.org/10.1063/5.0174480

30 November 2023 10:33:23

Effective control of electromagnetic waves is enabled by their interactions with matter. In this regard, immense efforts have been particularly exerted on the research on artificial material platforms and their ability to enhance manipulation of waves.[1–7] Recently, there has been a great interest in 'wave trapping' structures, which may facilitate enhanced field confinements vital for many microwave and photonic applications. Conventional structures with very high quality factors (Q-factors) are rather bulky and/or fully closed resonant cavities.[8–10] On the other hand, dielectric resonators, utilizing Mie resonances, are more compact, but their Q-factors are modest. Bound states in the continuum (BICs) represent an interesting approach toward open and high-Q systems.[11–17] BICs are exotic nonradiating modes found typically in periodic structures and specific multilayered structures made of extreme materials, such as epsilon-near zero materials. Although their Q-factors are theoretically infinite, practical systems only form quasi-BICs with finite Q-factors due to material absorption and finite sample size as well as structural disorder and defects. Still, quasi-BICs can be used to increase the Q-factor of a resonant system through cancelation of the radiative channels.

Quasi-BICs have been demonstrated in various structures at both microwave and optical frequencies. The main difference between optical and microwave BICs induced in arrays is the size. At microwave frequencies, the number of elements is usually limited to a few hundred for any practical purposes since the period is between a few millimeters to several centimeters.[18,19] This is, in general, not a problem for optical arrays where thousands of elements can be fitted within a few centimeters. As the Q-factor of a quasi-BIC scales with the number of elements, a different approach is needed for microwave quasi-BIC structures. Recently, it was demonstrated that the aspect ratio of a single cylindrical dielectric resonator can be tuned to induce strong mode coupling for either enhanced or suppressed scattering. In the suppressed regimes, supercavity modes are formed with physical roots closely associated with quasi-BICs.[17,20–22] An experimental Q-factor of 12 500 was achieved at microwave frequencies using a low-loss ceramic resonator with a relative permittivity of 44.8 and a loss tangent of 10^{-4}. Although the development of ceramic materials has increased the availability of ceramic resonators, their cost is still high.

A different approach toward a compact BIC structure has also been demonstrated.[23] In this work, the high conductivity of metals at microwave frequencies was exploited to simulate periodic boundary conditions, which was achieved with simple rectangular waveguides. The boundary-induced BIC was achieved by inserting a metallic resonator within the metallic walls of the waveguide, thus rendering an infinite periodic array. By breaking the symmetry of the resonator with tiny volumes of water, a quasi-BIC was excited and utilized for sensing tiny perturbations in the water. However, since the resonator is fully enclosed by the waveguide, the quasi-BIC can only be excited by the natural waveguide modes and not by free-space waves. In another work, quasi-BICs were demonstrated in configurations of rectangular waveguides coupled to cylindrical cavities operating in the high end of the microwave frequency spectrum.[24,25] Being restricted to waveguide configurations greatly limits the potential applications, and, thus, the

Published under an exclusive license by AIP Publishing

next natural step is to study how related concepts can be applied in free-space configurations. Such all-metallic resonators will be simple, robust, and low-cost alternatives to the costly ceramic resonators.[20–22]

The purpose of this work is to investigate a high-Q resonator, open to free-space waves, which is based on the principle of boundary-induced BIC. First, we show that a BIC, induced by an octupole mode, is supported in an array of metallic complementary asterisk-shaped resonators at around 5 GHz. In our case, the periodic conditions of the array can be simulated with metallic surfaces. Moreover, the high-order mode has highly confined fields, and, thus, the surrounding metallic surfaces supporting the required boundary conditions can be reduced to subwavelength sizes with minimal impact on the resulting Q-factor. In contrast, the resonator also supports BICs induced by low-order modes, which are highly affected by the size of the surrounding surfaces. These observations agree well with a theoretical study of BICs in multipolar lattices.[17] A prototype of the resonator is realized by milling its shape in a single block of aluminum. The prototype is investigated experimentally for both near- and far-field excitations, and a Q-factor of around 1500 is reported, mainly limited by material losses. The resonator holds several advantages, including its simplicity, robustness, and scalability, making it attractive for a wide range of applications where enhanced wave-matter interactions are required.

In the first part of the work, a square array of resonators is investigated numerically for operational frequency at around 5 GHz. The simulations are performed using COMSOL Multiphysics. A sketch of the single array element is shown in Fig. 1(a) and consists of a complementary eight-arm asterisk-shaped metallic resonator. The arms of the resonator produce poles in the local field of the resonator, and, thus, the employed eight-arm structure should naturally support an octupole mode. A two-arm (four-arm) structure would only support the dipole mode (both the dipole and quadrupole modes), whereas the eight-arm structure includes the octupole mode. The values of the geometric parameters are $a = 40$ mm $(0.7\lambda_0)$, $b = 36$ mm $(0.6\lambda_0)$, $c = 3$ mm $(0.05\lambda_0)$, and $d = 5$ mm $(0.08\lambda_0)$ with λ_0 being the free-space wavelength at 5 GHz. The geometrical parameters were adjusted to achieve an octupole mode sufficiently below the diffraction limit while still maintaining an acceptable Q-factor. The shape of the resonator facilitates three BICs originating from two quadrupole modes (4.7 and 4.9 GHz) and an octupole mode (5.2 GHz). When considering perfect electric conducting material, i.e., lossless material, the Q-factor is infinite at the Γ-point, corresponding to plane wave excitations at normal incidences. In Fig. 1(b), the Q-factor for the three BIC modes, obtained from the eigenmode analysis, is shown as a function of $k_x a/2\pi$ for y-polarized field, where k_x is the transverse wavenumber along the x-axis. The electric and magnetic fields are shown on the top of the single array element in Fig. 1(c). Mode 1 is highly susceptible to symmetry-breaking showing a rapidly decreasing Q-factor in Fig. 1(b), whereas mode 2 is far more robust to symmetry-breaking, mainly coming from the existence of an additional BIC at $k_x a/2\pi \approx 0.06$. However, mode 3 shows superior robustness, which is facilitated by a magnetic octupole with a high rotational symmetry.

Moving from the lossless, perfect conducting case, the results for copper elements with the conductivity $\sigma = 5.8 \times 10^7$ S/m are next discussed, see Fig. 1(b), which shows reduced Q-factors at a level of around 2500. Although the Ohmic losses in the metal significantly reduce the maximum Q-factor at the Γ-point, the symmetry-protection is conserved. For mode 3, the radiative leakage is smaller than the absorption for all incidence angles up to the diffraction limit ($k_x a/2\pi \approx 0.3$) making the Q-factor nearly constant. Thus, mode 3 will be greatly protected against disorders and perturbations even in the near field. This includes not only any geometrical variations along the array but also the truncation of the total array length. To further minimize the effect of truncation, highly conductive walls can be added around the sides of a single array element, which we refer to as "side walls," effectively emulating the periodic nature of the array and significantly reducing the size of the structure. In the case of resonators with low-order dipole modes, the near fields of these resonators are not very confined, and, thus, the side walls must be several wavelengths in extent, making the configuration closed to external excitations. However, resonators with high-order modes, like mode 3, have highly confined near fields, such that the side walls can be significantly reduced, effectively forming an open cavity mode or a so-called "super-cavity mode."

30 November 2023 10:33:23

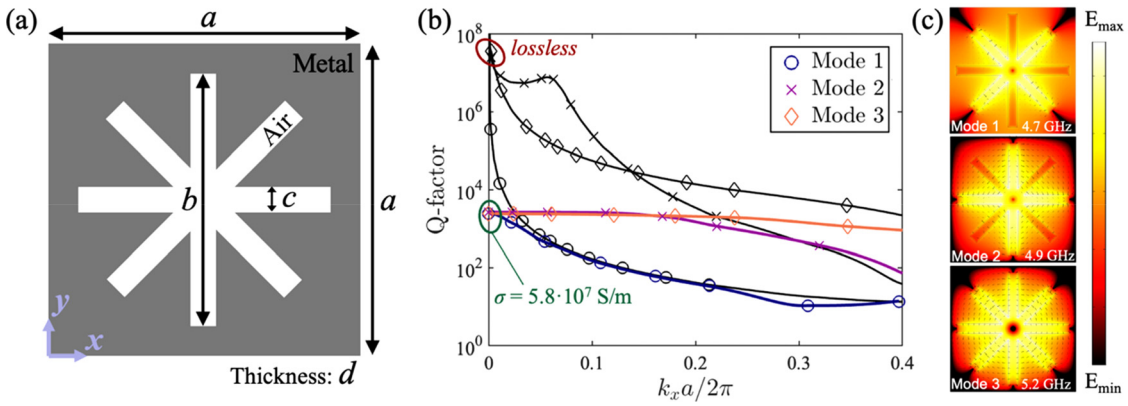

FIG. 1. The resonator in an array configuration. (a) Sketch of the cross-sectional view of the single array element: a metallic complementary eight-arm asterisk-shaped resonator with $a = 40$, $b = 36$, $c = 3$, and $d = 5$ mm. (b) Q-factor as a function of $k_x a/2\pi$ for the three BICs with and without metallic losses. The results are obtained from numerical eigenmode analyses using COMSOL Multiphysics. (c) The electric field magnitude (colors) and magnetic field (arrows) on the top surface of the resonator for each mode ($k_x a/2\pi = 0$). Both fields are shown in logarithmic scale.

Published under an exclusive license by AIP Publishing

To this end, a single array element with conductive walls on its sides is investigated. A sketch of the configuration is shown in Fig. 2(a). The thickness of the walls is 2 mm ($0.03\lambda_0$), and closed/open resonators are considered with/without top and bottom plates. As in the previous case, the three modes are identified from the eigenmodes analyses, and the resulting Q-factors are shown in Fig. 2(b) as functions of the sidewall length for the open resonator without material losses. The Q-factor of the closed resonator without material losses is infinite for all modes since there is no absorption or radiation leakage. As expected, mode 3 manifests far better protection against shortening of the side walls compared to the two other modes. With a sidewall length of 12 mm ($0.2\lambda_0$), mode 3 is effectively a supercavity mode with a Q-factor of 12 000. The electric far-field pattern of mode 3 is shown in Fig. 2(c) and is found to resemble a magnetic octupole mode of the corresponding spherical wave expansion.[26,27] Including metallic losses ($\sigma = 5.8 \times 10^7$ S/m), see Fig. 2(d), the maximum Q-factor is reduced to around 2000. The results for both open and closed resonators are included in Fig. 2(d). In this regard, it must be mentioned that the Q-factor of a closed cavity without the asterisk-shaped element is higher (around 8000 for the TE_{101} mode). However, if one of the metallic walls is removed, the mode vanishes. Thus, the confinement mechanism, as well as the applicational aspects, of the closed cavity is very different from the one of the open cavity. When the sidewall length is less than $0.25\lambda_0$, the reduced space in the closed resonator highly affects the modes, consequently decreasing their Q-factors. This is not the case for the open resonator, where the Q-factor of mode 3 is still high for sidewall lengths below $0.2\lambda_0$. In addition, the effect of the material losses on the Q-factor of mode 3 is shown in Fig. 2(e) exhibiting a significant change in the Q-factor, thus a possible way to tune the resonator.

A prototype of the open resonator was fabricated from a single aluminum block in which the walls and asterisk shapes were milled. A photograph of the resonator is shown in Fig. 3(a). Its scattering properties were tested in the DTU Electromagnetic Test Centre scattering test facility using the bistatic measurement setup shown in Fig. 3(b). Two C-band horn antennas connected to a Keysight PNA-L network analyzer were used to transmit an incident wave and collect the scattered field from the resonator. Typical scattering quantities, such as the differential cross section (dSCS) and the extinction cross section (ECS), will be used to experimentally characterize the performance of the proposed open resonator. The dSCS (m^2) describes the amount of power of the incident power density that is scattered in different directions, whereas ECS (m^2) describes the total power that is extinct (scattered + absorbed) from the incident wave.[28] Using the method of substitution, these scattering quantities will be determined from the measured S-parameters.[29–31] In this work, the dSCS is calculated and measured in the opposite (backward) and the same (forward) directions from which the wave is incident. First, the experimental setup and method were validated by measuring metallic spheres with well-known scattering characteristics, and the measurement results were found to show great consistency and acceptable accuracy. It must be mentioned that the resonator has a much higher Q-factor than those of metallic spheres, and, therefore, its scattering is more difficult to isolate from the clutter and additional scattering due to the antennas and tripods. An analysis of the isolation, as well as the measurement results for the metallic spheres, can be found in the supplementary material.

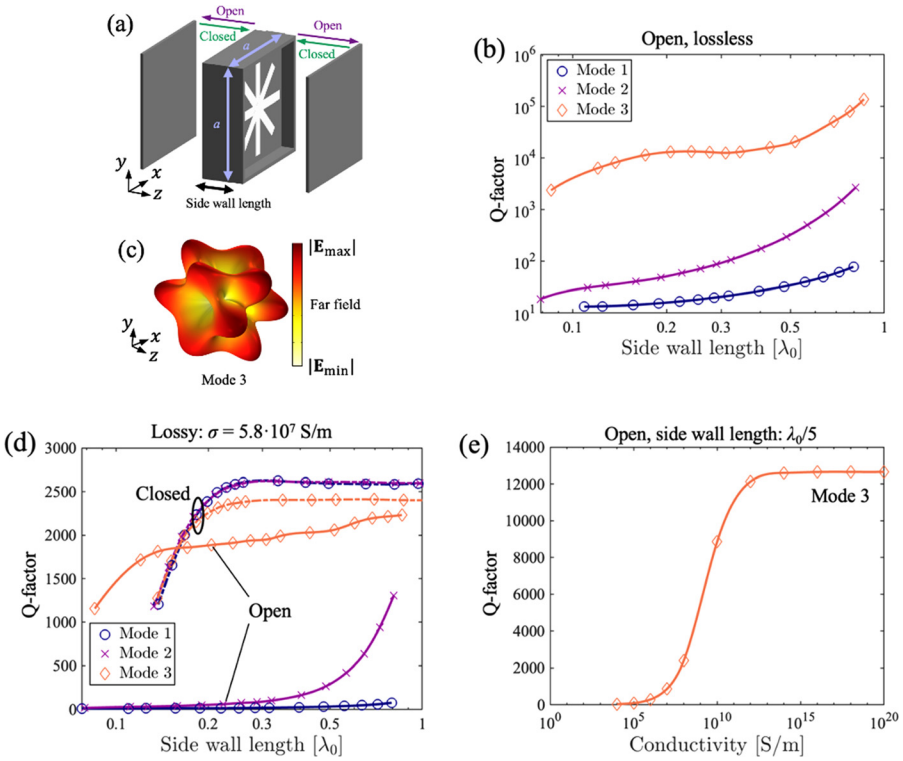

FIG. 2. The single resonator with side walls. (a) Sketch of the single metallic resonator in closed and open configurations. The thickness of the side walls is 2 mm, and the other geometrical parameters are the same as in Fig. 1. (b) Q-factor as a function the sidewall length for the three modes of the open and lossless resonator. (c) Electric far-field pattern of mode 3 for the open resonator with sidewall length 12 mm and resonance frequency 5.2 GHz. (d) Q-factor as a function of the sidewall length for both the closed and open resonators made of copper. (e) Q-factor of mode 3 as a function of the conductivity for the resonators with a sidewall length of 12 mm.

30 November 2023 10:33:23

Published under an exclusive license by AIP Publishing

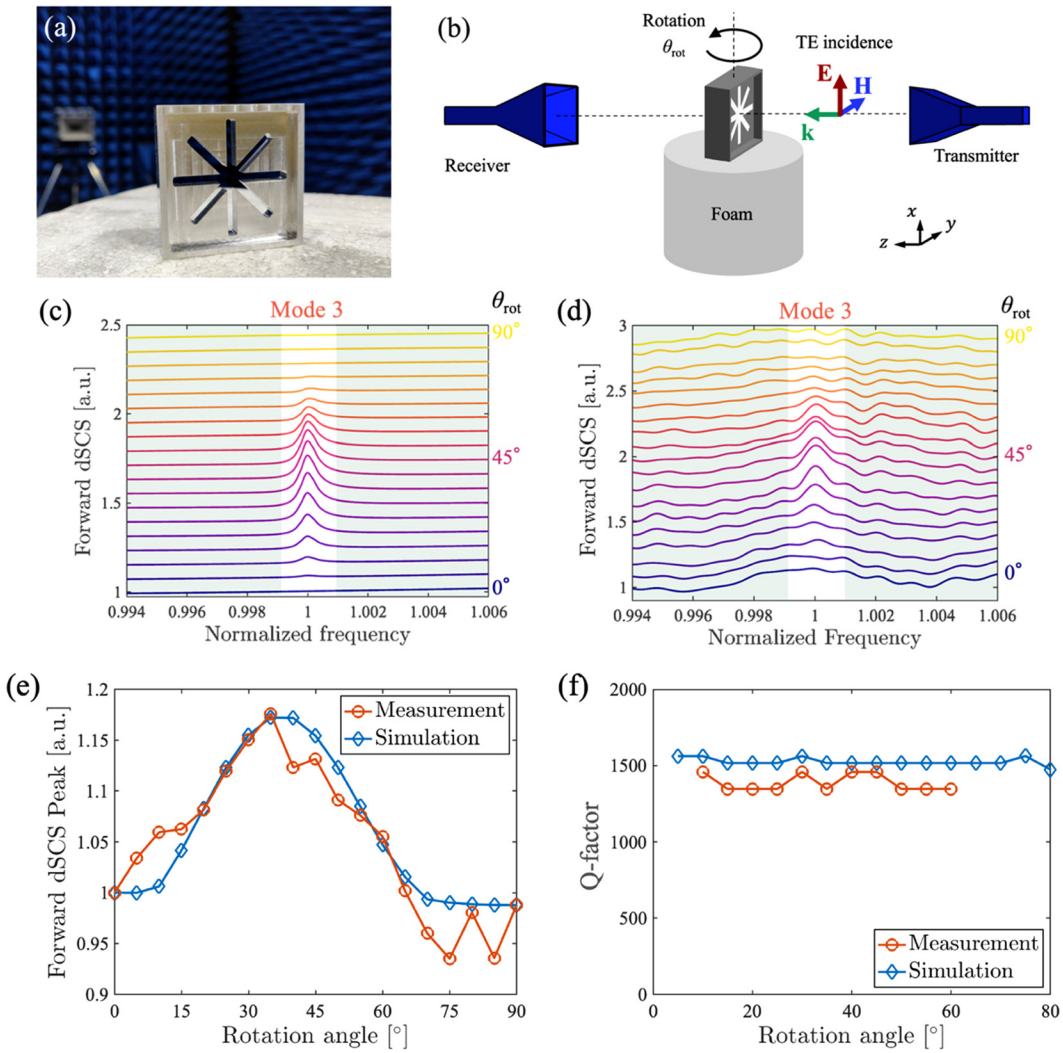

FIG. 3. Far-field characterization of the single resonator with side walls. (a) Photograph of the fabricated resonator made of aluminum. (b) Sketch of the experimental far-field scattering setup. (c) Simulated and (d) measured forward differential scattering cross sections (dSCS) as functions of the normalized frequency, f/f_r with f_r being the resonance frequency, for the different rotation angles of the resonator. Simulated and measured (e) forward dSCS peak and (f) Q-factor as functions of the rotation angle.

The scattering was measured for different incidence angles by rotating the resonator around the axis parallel to the incident electric field, see Fig. 3(b). The forward dSCS, obtained from the simulations and measurements, is shown in Figs. 3(c) and 3(d), as a function of the normalized frequency and for different rotation angles from 0° to 90°. The results for the corresponding backward dSCS and the ECS, showing very similar behavior, are included in the supplementary material. For the rotation angle $\theta_{rot} = 0°$, corresponding to normal incidence, mode 3 (the supercavity mode) is not excited as the wave is propagating along a nodal line of the magnetic octupole mode. However, for oblique angles, the mode is excited causing a peak in the measured scattered field at around 5.2 GHz. The simulated and measured scattering peak is shown in Fig. 3(e) as a function of the rotation angle exhibiting great agreement. The average relative deviation between the simulated and measured normalized scattering peak is around 2.1%. The scattering peak is maximum at $\theta_{rot} = 35°$, whereas the minima are at $\theta_{rot} = 0°$ and $\theta_{rot} = 90°$. Moreover, the Q-factor shown in Fig. 3(f) as a function of the rotation angle also presents very good agreement between the simulations and measurements. The Q-factors have been calculated by taking the ratio of the frequency of the forward dSCS peak (f_r) and the full width half maximum (Δf). The Q-factor for the aluminum resonator is slightly lower (around 1500) compared to the copper resonator (see Fig. 2), which is due to the slightly lower conductivity of aluminum (3.6×10^7 S/m). Still, the resonator shows great protection against symmetry-breaking by the minimal change between different rotation angles.

The resonator was also characterized in the case of near-field excitation using a simple loop antenna, see the sketch of the setup in Fig. 4(a). The loop antenna (port 1) was connected to a network analyzer, and a C-band horn antenna (port 2) was used to measure the

30 November 2023 10:33:23

Published under an exclusive license by AIP Publishing

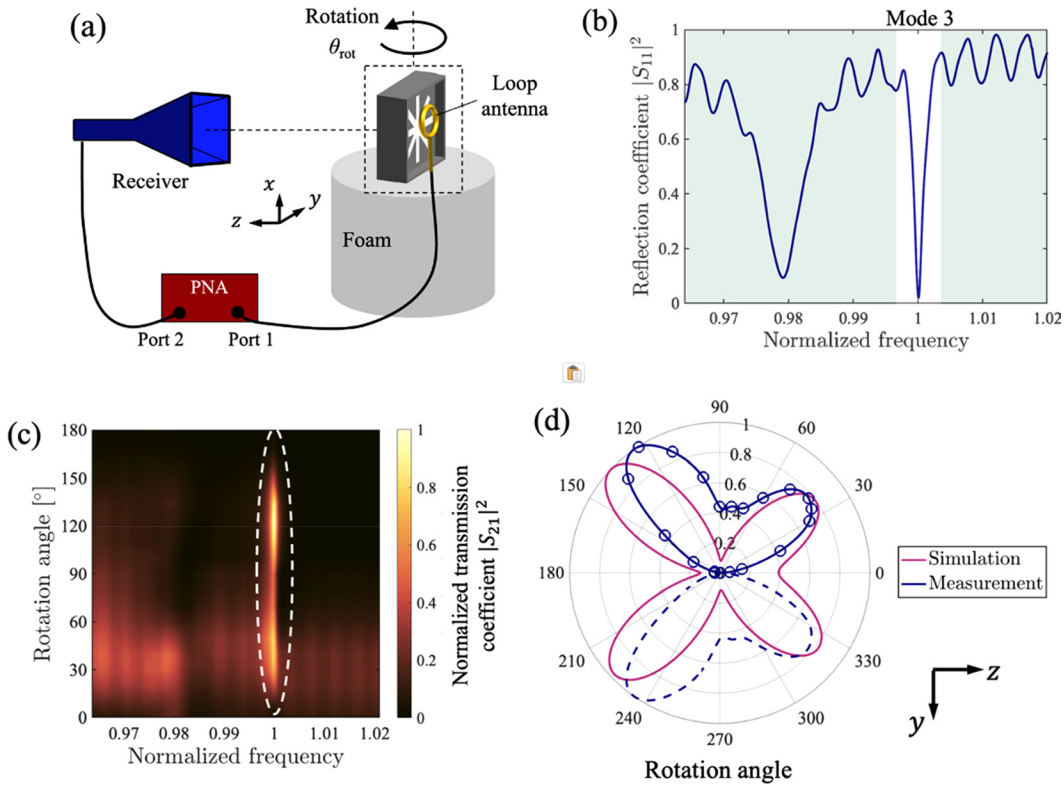

FIG. 4. Near-field characterization of the single resonator with side walls. (a) Sketch of the near-field excitation of the resonator using a small loop antenna. (b) Measured reflection coefficient S_{11} as a function of the normalized frequency f/f_r with f_r being the resonance frequency. (c) Measured normalized transmission coefficient S_{21} as a function of the normalized frequency and rotation angle. (d) Simulated and measured normalized $|S_{21}|^2$ at the resonance frequency as a function of the rotation angle. The resonance frequency is 5.24 GHz, and the Q-factor is 650.

radiated field. The resonator and loop antenna were rotated from 0° to 180° in a similar way as in the experimental setup in Fig. 3(b). The measured reflection coefficient (S_{11}) is shown in Fig. 4(b) as a function of the normalized frequency. The loop antenna is highly coupled to the octupole mode of the resonator causing a significant reduction of the reflection coefficient around the resonance frequency. However, the coupling also affects the Q-factor, which is reduced to 650. A second resonance is observed at lower frequencies, which has a lower Q-factor and intensity. A minimal change between different rotation angles was observed for the S_{11} showing good stability of the experimental setup, see the supplementary material. The measured normalized transmission coefficient (S_{21}) is shown in Fig. 4(c) as a function of the normalized frequency and the rotation angle. There are two strong transmission peaks at two different rotation angles coming from the excited supercavity mode (mode 3). In fact, the radiation intensity is much higher than the other resonance found at lower frequencies, thus demonstrating the applicability of the resonator in antenna configurations. The two transmission peaks are also found in Fig. 4(d), where the measured and simulated radiation patterns are shown at the resonance frequency. Four lobes are measured in the scanned *zy*-plane, which agrees well with the simulations and the 3D far-field scattering from the eigenmode analysis in Fig. 2(c).

In this work, the concept of a supercavity mode in a purely metallic resonator was demonstrated. The supercavity mode was achieved with an octupole mode facilitated by an eight-arm asterisk-shaped resonator. The resonator was surrounded by metallic walls on its sides to induce periodic conditions and effectively boost the Q-factor. Utilizing the highly confined fields of the octupole mode, the side walls were reduced to subwavelength sizes, thus minimizing the overall footprint of the resonator and making it open to external excitations. A prototype of the resonator made in aluminum was fabricated and tested experimentally for both near- and far-field excitations. An experimental Q-factor of around 1500 was achieved mainly limited by the aluminum losses. The resonator design is very simple, which enabled a straightforward fabrication of the prototype: the asterisk-shape and walls were simply milled out in a single square block of aluminum. Thus, the fabrication can easily be upscaled and is even suitable for additive printing techniques, with the only requirement being that highly conductive materials are used. In addition, it must be emphasized that the resonator design can easily be scaled for other operational frequencies. In addition to its simplicity, the resonator has several other advantages. Its solid and homogeneous form makes it very robust. Moreover, it can easily be extended to an array of multiple resonators. In particular, its complementary form makes it suitable for metasurfaces engineered for transmission. However, it can also be used as a gas sensor since gas is able to naturally flow through it. Thus, the resonator is attractive for many applications where enhanced wave-matter interactions are of prime importance, including advanced functional material designs, energy harvesting as well as sensing.

30 November 2023 10:33:23

Published under an exclusive license by AIP Publishing

See the supplementary material for details of figures and discussion of the scattering measurement of metallic spheres, figures of the simulated and measured backward differential scattering cross section and the extinction cross section as well as the measured reflection coefficient for all rotation angles for the resonator, and the definitions of different parameters.

The authors would like to thank the workshop at the Division for Electromagnetic Systems, Technical University of Denmark, for the fabrication of the resonator prototype used in the experiment. The authors also thank M.Sc. Engineer Jeppe Majlund Bjùrstorp for the assistance in the experimental work.

AUTHOR DECLARATIONS

Conflict of Interest

The authors have no conflicts to disclose.

Author Contributions

Rasmus E. Jacobsen: Conceptualization (equal); Formal analysis (equal); Investigation (lead); Methodology (lead); Validation (lead); Writing – original draft (lead); Writing – review & editing (equal). **Samel Arslanagić:** Conceptualization (equal); Formal analysis (equal); Investigation (supporting); Methodology (supporting); Supervision (lead); Writing – original draft (supporting); Writing – review & editing (equal).

DATA AVAILABILITY

The data that support the findings of this study are available from the corresponding author upon reasonable request.

REFERENCES

[1]S. B. Glybovski, S. A. Tretyakov, P. A. Belov, Y. S. Kivshar, and C. R. Simovski, "Metasurfaces: From microwaves to visible," Phys. Rep. **634**, 1–72 (2016).
[2]N. Yu and F. Capasso, "Flat optics with designer metasurfaces," Nat. Mater. **13**(2), 139–150 (2014).
[3]S. Jahani and Z. Jacob, "All-dielectric metamaterials," Nat. Nanotechnol. **11**(1), 23–36 (2016).
[4]R. E. Jacobsen, S. Arslanagić, and A. V. Lavrinenko, "Water-based devices for advanced control of electromagnetic waves," Appl. Phys. Rev. **8**(4), 041304 (2021).
[5]A. Grbic and S. Maci, "EM Metasurfaces [Guest Editorial]," IEEE Antennas Propag. Mag. **64**(4), 16–22 (2022).
[6]A. Monti, A. Alù, A. Toscano, and F. Bilotti, "Design of high-Q passband filters implemented through multipolar all-dielectric metasurfaces," IEEE Trans. Antennas Propag. **69**(8), 5142–5147 (2021).
[7]A. Rahimzadegan, D. Arslan, D. Dams, A. Groner, X. Garcia-Santiago, R. Alaee, I. Fernandez-Corbaton, T. Pertsch, I. Staude, and C. Rockstuhl, "Beyond dipolar Huygens' metasurfaces for full-phase coverage and unity transmittance," Nanophotonics **9**(1), 75–82 (2020).
[8]N. Toropov, G. Cabello, M. P. Serrano, R. R. Gutha, M. Rafti, and F. Vollmer, "Review of biosensing with whispering-gallery mode lasers," Light: Sci. Appl. **10**(1), 42 (2021).
[9]K. J. Vahala, "Optical microcavities," Nature **424**(6950), 839–846 (2003).
[10]R. A. Alahnomi, Z. Zakaria, Z. M. Yussof, A. A. Althuwayb, A. Alhegazi, H. Alsariera, and N. A. Rahman, "Review of recent microwave planar resonator-based sensors: Techniques of complex permittivity extraction, applications, open challenges and future research directions," Sensors **21**(7), 2267 (2021).
[11]C. W. Hsu, B. Zhen, A. D. Stone, J. D. Joannopoulos, and M. Soljačić, "Bound states in the continuum," Nat. Rev. Mater. **1**(9), 16048 (2016).
[12]K. Koshelev, G. Favraud, A. Bogdanov, Y. Kivshar, and A. Fratalocchi, "Nonradiating photonics with resonant dielectric nanostructures," Nanophotonics **8**(5), 725–745 (2019).
[13]S. C. Malek, A. C. Overvig, A. Alù, and N. Yu, "Multifunctional resonant wavefront-shaping meta-optics based on multilayer and multi-perturbation nonlocal metasurfaces," Light: Sci. Appl. **11**(1), 246 (2022).
[14]A. Overvig, N. Yu, and A. Alù, "Chiral quasi-bound states in the continuum," Phys. Rev. Lett. **126**(7), 073001 (2021).
[15]Z. Yu and X. Sun, "Acousto-optic modulation of photonic bound state in the continuum," Light: Sci. Appl. **9**, 1 (2020).
[16]A. F. Sadreev, "Interference traps waves in an open system: Bound states in the continuum," Rep. Prog. Phys. **84**(5), 055901 (2021).
[17]S. Gladyshev, A. Shalev, K. Frizyuk, K. Ladutenko, and A. Bogdanov, "Bound states in the continuum in multipolar lattices," Phys. Rev. B **105**(24), L241301 (2022).
[18]Y. Xie, Z. Zhang, Y. Lin, T. Feng, and Y. Xu, "Magnetic quasi-bound state in the continuum for wireless power transfer," Phys. Rev. Appl. **15**(4), 044024 (2021).
[19]Z. F. Sadrieva, M. A. Belyakov, M. A. Balezin, P. V. Kapitanova, E. A. Nenasheva, A. F. Sadreev, and A. A. Bogdanov, "Experimental observation of a symmetry-protected bound state in the continuum in a chain of dielectric disks," Phys. Rev. A **99**(5), 053804 (2019).
[20]M. V. Rybin, K. L. Koshelev, Z. F. Sadrieva, K. B. Samusev, A. A. Bogdanov, M. F. Limonov, and Y. S. Kivshar, "High-*Q* supercavity modes in subwavelength dielectric resonators," Phys. Rev. Lett. **119**(24), 243901 (2017).
[21]M. Odit, K. Koshelev, S. Gladyshev, K. Ladutenko, Y. Kivshar, and A. Bogdanov, "Observation of supercavity modes in subwavelength dielectric resonators," Adv. Mater. **33**(1), 2003804 (2021).
[22]K. Koshelev, S. Kruk, E. Melik-Gaykazyan, J. H. Choi, A. Bogdanov, H. G. Park, and Y. Kivshar, "Subwavelength dielectric resonators for nonlinear nanophotonics," Science **367**(6475), 288–292 (2020).
[23]R. E. Jacobsen, A. Krasnok, S. Arslanagić, A. V. Lavrinenko, and A. Alú, "Boundary-induced embedded eigenstate in a single resonator for advanced sensing," ACS Photonics **9**(6), 1936–1943 (2022).
[24]G. Annino, H. Yashiro, M. Cassettari, and M. Martinelli, "Properties of trapped electromagnetic modes in coupled waveguides," Phys. Rev. B **73**(12), 125308 (2006).
[25]G. Annino, M. Cassettari, and M. Martinelli, "A new concept of open TE_{011} cavity," IEEE Trans. Microwave Theory Tech. **57**(1), 775–783 (2009).
[26]W. W. Hansen, "A new type of expansion in radiation problems," Phys. Rev. **47**(2), 139 (1935).
[27]J. A. Stratton, *Electromagnetic Theory* (Wiley-IEEE Press, 2015).
[28]C. F. Bohren and D. R. Huffman, *Absorption and Scattering of Light by Small Particles*, 1st ed. (John Wiley & Sons, Hoboken, NJ, 1983).
[29]R. E. Jacobsen, A. V. Lavrinenko, and S. Arslanagić, "Reconfigurable dielectric resonators with imbedded impedance surfaces—From enhanced and directional to suppressed scattering," Appl. Phys. Lett. **122**(8), 81701 (2023).
[30]E. F. Knott, *Radar Cross Section Measurements*, 1st ed. (Springer, New York, 1993).
[31]C. Larsson and M. Gustafsson, "Wideband measurements of the forward RCS and the extinction cross section," Appl. Comput. Electromagn. Soc. J. **28**(12), 1145–1152 (2013).

30 November 2023 10:33:23

Published under an exclusive license by AIP Publishing